The Thesis Committee for Woongsoon Choi
Certifies that this is the approved version of the following thesis:

Characterization of D135 Group II Intron Ribozyme Dimerization

APPROVED BY
SUPERVISING COMMITTEE:

Supervisor:

Rick Russell

Alan Lambowitz

Characterization of D135 Group II Intron Ribozyme Dimerization

by

Woongsoon Choi, B.S.Bioch.

Thesis

Presented to the Faculty of the Graduate School of

The University of Texas at Austin

in Partial Fulfillment

of the Requirements

for the Degree of

Master of Arts

The University of Texas at Austin

May 2013

Dedication

Dedicated to my wife and my parents

Acknowledgements

Most importantly, I would like thank my advisor Rick Russell for his guidance and coaching throughout the program. I definitely learned a lot from his logical and critical scientific thinking. His clear and patient supervision on my work was the most instrumental tool for lubricating my work. Also, I would like to thank Alan Lambowitz for reading my thesis. In addition, I want to give special thank to Pilar Tijerina for her initial assistance to settle in the lab, and to Inga Jarmoskaite for helping me with small-angle X-ray scattering and many useful discussions. I also want to thank the former and current Russell lab members: Brian Cannon, Brant Gracia, David Mitchell, Cynthia Pan, Jeff Potratz, Yaqi Wan, and Luke Ward.

Abstract

Characterization of D135 Group II Intron Ribozyme Dimerization

Woongsoon Choi, M.A.

The University of Texas at Austin, 2013

Supervisor: Rick Russell

Group II introns are highly structured RNAs that carry out self-splicing reactions. The multiple turnover version of one of these introns, termed the D135 ribozyme, is derived from the mitochondrial aI5γ intron of *Saccharomyces cerevisiae* and is widely studied as a model RNA for group II intron folding. An important current goal is to probe global changes during its folding with or without DEAD-box chaperone proteins. My initial experiments to study global compaction using small angle X-ray scattering (SAXS) of D135 reveal rapid initial compaction. Unexpectedly, slower increases in R_g value and forward scattering were observed and shown to result from dimerization of the ribozyme. Dimerization was also observed with native electrophoretic mobility shift assays. Here, I have characterized the dimerization process at various conditions. Dimerization requires Mg^{2+}, with similar concentration dependence as tertiary folding, and the dimer is efficiently disrupted by the ATP-dependent activity of DEAD-box proteins. Dimerization does not affect ribozyme catalysis, as both the monomer and the dimer are shown to be fully active. Further experiments showed that dimerization results from duplex formation by an artificial 3' tail that has extensive self-complementarity, as

the deletion of this tail ablates dimerization. Constructs lacking this artificial 3' tail are likely to simplify further study of the folding process of this ribozyme.

Table of Contents

List of Tables ix

List of Figures x

List of Illustrations xi

Chapter 1: Introduction 1

Chapter 2: Results and Discussion 5

2.1 Observation of the D135 dimer by SAXS and native gel approaches under the non-physiological conditions 5

2.2 Dimerization under the near-physiological condition and disruption of dimers by DEAD-box proteins 8

2.3 D135 dimerization does not affect its catalysis 10

2.4 Time-resolved SHAPE Footprinting to probe the dimerization interface 12

2.5 Artificial 3' tail mediates the dimerization 13

2.6 Discussion 14

Chapter 3: Materials and methods 27

3.1 RNA preparation 27

3.2 Protein purification 27

3.2 Equilibrium and time-resolved SAXS measurement 27

3.3 Native gel electrophoretic mobility shift assay for monitoring dimerization equilibrium and kinetics 28

3.4 Multiple turnover catalytic activity and folding Assay 30

3.5 Benzoyl cyanide SHAPE footprinting 31

Appendix 33

References 34

List of Tables

Table 2.1 Guinier analysis for time-resolved SAXS 16

Table 2.2 Dimerization observed by native gel at the non-physiological condition16

Table 2.3 Dimerization observed by native gel at the near-physiological condition16

Table 2.4 Dimer dissociation at the near-physiological condition 16

Table 2.5 Continuous folding assay and prefolded D135 control at various [D135]17

Table 2.6 Comparison between dimerization rate and catalysis rate.....17

Table 2.7 Rate constants calculated from time-resolved SHAPE footprinting 17

List of Figures

Figure 1 Secondary structures and identified tertiary contacts of ai5γ intron and D135 ribozyme. 4

Figure 2.1 Time resolved SAXS at the non-physiological condition 18

Figure 2.2 Observation of dimerization by native gel at the non-physiological condition 19

Figure 2.3 Magnesium requirements for ribozyme compaction and dimerization.20

Figure 2.4 Time resolved SAXS at the near-physiological condition 21

Figure 2.5 Dimerization and dissociation of dimers at the near-physiological condition and active disruption of dimers by DEAD-box proteins. .22

Figure 2.6 Effect of dimerization on catalysis 23

Figure 2.7 Time-resolved SHAPE footprinting 24

Figure 2.8 The 3'-tail mediates dimerization.....25

Figure A.1 Dimerization at the near-physiological condition with differently prepared D135 ribozymes 33

List of Illustrations

Illustration 2.1 Reaction schemes 26

Chapter 1: Introduction

Group II introns are self-splicing ribozymes present in diverse organellar genomes of fungi and plants as well as many bacterial genomes. These introns gained much interest from researchers as they were proposed to be an evolutionary ancestor for the spliceosomes and nuclear introns. The rationale behind this hypothesis is that their splicing mechanism is practically the same as the two-step transesterification mechanism of spliceosomal splicing reaction: the 2'-OH group of the bulged adenosine attacks 3' end of the 5'exon, and then the 5' and 3' exons are ligated. [1] This hypothesis is further supported when the capability of the group II intron in retrohoming and retrotransposition was discovered. The spliced intron species with a help of intron-encoded proteins can insert itself to an intron-less version of the same gene or completely different genes.

Like other large ribozymes, group II introns must fold into specific functional structures to carry out catalysis. Shortly after their discovery, the secondary structures of group II introns were proposed from comparative analysis of phylogenetically conserved group II introns. All group II introns have six domains that branch out from central helical junctions. (**Figure 1A**) Domain 1 (DI) is the largest one that serves as the docking platform for the rest of the domains. Domain 5 (DV) is the catalytic center, which coordinates catalytically important metal ions. Domain 6 (DVI) contains the bulged adenosine, which serves as the nucleophile for the first step of splicing. Domain 3 (DIII) contains a structurally important region, and domain 2 (DII) is important for structural rearrangement. Domain 4 (DIV) may contain the open reading frame that encodes the protein with maturase and reverse transcriptase domain that is necessary for retrohoming and retrotransposition activity of group II intron. Many long range tertiary contacts were identified using experimental methods by many different groups.[1] Recently solved crystal structures of the *Oceanobacillus iheyensis* group II intron, which is classified in the smallest lineage of group II introns, confirmed many of the proposed tertiary contacts that are common in all group II intron lineages.[2]

The folding process of group II introns has been largely studied with the multiple-turnover ribozyme version of *S. cerevisiae COX1* gene intron ai5γ.[3,4] This ribozyme version contains the catalytically important domains for splicing: DI, DIII, and DV. (**Figure 1B**) This ribozyme is called D135, and it can cleave an RNA oligonucleotide composed of 17-nt of 5'-exon sequence and the first 7-nt of 5' end of the intron so that the cleavage reaction mimics the first step of splicing. The initial characterization of this ribozyme folding was performed at a non-physiological condition with an elevated temperature and high magnesium and potassium concentration where the *in vitro* splicing reaction is favored.[3,4] Numerous studies indicate that the folding of D135 at this condition follows apparent two-step kinetics as all tertiary structures are formed more or less at the same time with rate constant of 1 to 2 min^{-1}, monitored by hydroxyl radical footpringting.[5] Parallel native gel experiments and catalytic activity assay show that global compaction and ribozyme activity occur at the same time, meaning that D135 ribozyme folds to a compact, native state upon folding of tertiary contact, directly without rate-limiting kinetic traps.[6,7] The rate-limiting step of D135 folding is suggested to lie within the folding of DI, as folding of DI itself follows the same Mg^{2+} dependency and folding kinetics, which is then followed by fast DIII and DV docking.[7] However, it is still unclear whether this intermediate of fully folded DI and undocked DIII and DV is an obligate on-path intermediate. An alternative model is that DI and DIII fold around DV without forming the above intermediate.

The folding of D135 at more physiologically relevant condition for yeast growth is shown to be very different. Although the folding pathway to the native state is simple and direct at the non-physiological condition, the folding pathway of D135 in near-physiological condition is much slow or multi-phasic, with many folding pathways and kinetic traps. Under these conditions, complete folding of DI proceeds extremely slowly, but DIII and DV cannot dock in a stable manner at Mg^{2+} concentration lower than 10 mM.[8] As a result, the catalytic activity of folded D135 under the near-physiological condition is much lower than native state, which is folded under non-physiological condition.[8]

It is possible the slow folding of DI may be due to the presence of one or more long-lived misfolded conformations that must be disrupted to allow folding to native state. As the slow native folding caused by kinetic traps are resolved by DEAD-box proteins, the folding of both ai5γ intronic version and D135 ribozyme is facilitated by DEAD-box proteins both *in vivo* and under near-physiological condition *in vitro*.[9,10] The ATP-dependent duplex-unwinding activity is indicated to be essential for facilitating the native folding. ATP-independent activity of DEAD-box proteins has also been suggested to be important in folding of D135, but it is most likely important for compaction of DI as shown by nucleotide analogue interference mapping and single molecule fluorescence resonance energy transfer.[11,12]

Here, I initially attempted to follow the global compaction events of D135 ribozyme under both non- and near-physiological conditions and how DEAD-box proteins affect its compaction during the course of D135 folding by utilizing small angle X-ray scattering (SAXS). However, SAXS data unexpectedly revealed that D135 ribozymes dimerize. Dimerization of D135 can also be monitored in electrophoretic mobility shift assays. In this study, I investigated the possible implications of dimerization process during its function and whether general RNA chaperone protein can dislocate dimers. The dimerization is concentration dependent, and it does not have to be disrupted nor required for catalysis. Interestingly, ATP-dependent unwinding activity of DEAD-box proteins can disrupt D135 dimers. SHAPE footprinting shows that most native tertiary contacts are formed in the dimerization condition. Further experiments show that the dimerization of D135 is at the 3' end, which has a significant self-complementarity mediated by an artificially added sequence by the construct designers. Deletion of this sequence abolished the capability of dimerization. This study characterizes the dimerization process, and it suggests researchers to be aware of this process during their study of this ribozyme.

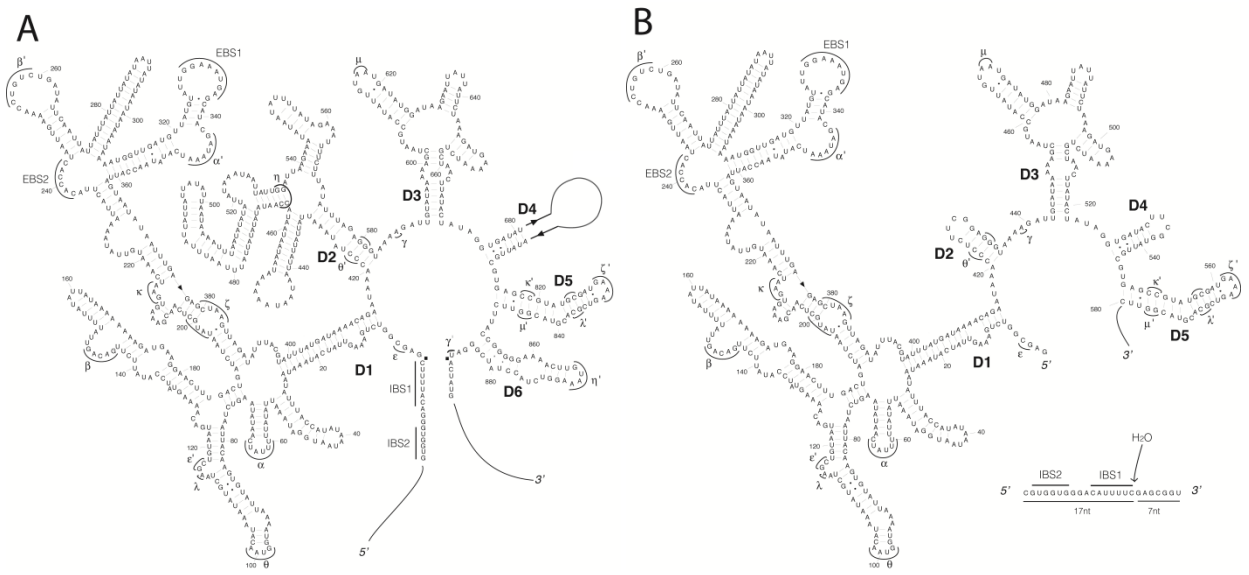

Figure 1 Secondary structures and identified tertiary contacts of ai5γ intron and D135 ribozyme.

(A) *S. cerevisiae COX1* gene intron ai5γ secondary structure. Domains are labeled with bold letters of "D" and roman numerals. Long-range tertiary contact partners are labeled with Greek letters and the prime of them. Sequences that guide exon and intron interaction are labeled as EBS (exon binding sequence) and IBS (intron binding sequence). (B) D135 multiple turnover ribozyme version. D2 and D4 are replaced with UUCG tetraloop. 35-nucleotide 3'-tail is denoted by a line. 24-nucleotide D135 substrate is shown below of D135 secondary structure. The arrow indicates the cleavage site.

Chapter 2: Results and Discussion

2.1 Observation of the D135 dimer by SAXS and native gel approaches under the non-physiological conditions

Small-angle X-ray scattering (SAXS) is a powerful method used to monitor changes in global shape, size, and oligomeric state of various biological macromolecules including RNA.[13,14] To monitor the rate of global compaction, I first performed time-resolved SAXS on D135 folding with a rapid flow mixer at the non-physiological condition (1 μM D135, 100 mM $MgCl_2$, 500 mM KCl, 42˚C). Kratky plot shows a very fast, unresolved compaction, which presumably includes an electrostatic relaxation (< 3 sec),[15] that is followed by a gradual increase of globular characteristic. (**Figure 2.1A**) Guinier approximation shows the radius of gyration (R_g) increases from 62 Å to 72 Å with a rate of 0.6 min^{-1} while the intensity at zero angle, I(0), increases by 1.9-fold. (**Figure 2.1B and C**) (**Table 2.1**) Unfortunately, the radius of gyration of the unfolded sample, which would serve as the initial point, was not able to be determined as the scattering of X-ray was poor. Only a reasonable estimate of R_g of the unfolded D135 comes from another hydrodynamic radius: Stokes Radius (R_h) determined from analytical ultracentrifugation experiment.[6] If the assumption that R_g of the first time point resembles the same compactness as the fully folded ribozyme whose R_h was reported as 61.4 Å, R_h and R_g has a 1:1 relationship. Thus, I assumed R_g of the unfolded D135 ribozyme would be approximately the same as its R_h, which is about 146 Å.[6] Therefore, R_g decreased approximately from 146 Å to 62 Å in a time scale shorter than 3 seconds. Collectively, both Kratky plot and R_g analysis demonstrates that there was rapid compaction, including electrostatic relaxation.

However, the slow increase of R_g and I(0) value was unexpected as I(0) should stay the same, and R_g should not increase as it is counter-intuitive to imagine the size of RNA becomes larger as it folds. The simplest explanation that accounts for the gradual increase in R_g value is that D135 molecules were enlarged by self-association to an oligomeric state. As the I(0) value is proportional to the square of the molecular weight and the concentration,[13] the near two-fold increase in I(0) is a clear evidence that D135 was forming a dimer because its molecular weight

was doubled while the concentration was halved. This time-resolved experiment suggests that dimerization was occurring at a similar time scale of the native folding of D135 (~1 min^{-1}).

Next, I looked for possible previous evidence of dimerization of D135. Dimerization of D135 was first observed by Pyle and colleagues with analytical ultracentrifugation.[6] When folded at the non-physiological condition for 15 minutes, two species of D135 with different sedimentation coefficients were observed, and their levels change depending on D135 concentrations. Under their investigation with linear regression, the dimer was formed with a K_d of about 10 nM. However, the authors only made an assertion that D135 dimer is catalytically active with no obvious experimental support, and they did not investigate further.

I next wanted to test if the rate of D135 dimerization is concentration-dependent as one may expect that the kinetics of a simple dimerization reaction is dependent on the concentration of monomers. To observe the concentration dependency, SAXS has a limited capability because a certain amount of RNA concentration is required for producing enough scattering of X-ray. Therefore, I next tested if the dimerization process could be monitored by the native gel electrophoresis with an assumption that the dimer complex is stable enough to be retained in the gel. First, I measured the equilibrium constant for dimerization under the non-physiological condition after folding for 1 hour. Monomer and dimer can be separated by 8% PAGE with 10 mM $MgCl_2$ after 3-hour separation at 300 V. The fraction of dimer was quantified as the D135 was either 5' or 3' end-labeled with ^{32}P, and the dimer fractions at different concentrations were fitted into the quadratic equation. (See Chapter 3.3) The K_d value was around 2-8 nM, which approximately agreed with the value from analytical ultracentrifugation (K_d = ~10 nM).[6] (**Figure 2.2A**)

I next measured the kinetics of dimerization at the non-physiological condition at 3 different concentrations of D135. Because it was not straightforward to separate the folding and dimerization steps, the experiment was designed to proceed from unfolded-monomer to folded-dimer. The simplest quench that could be used was to dilute D135 by 50- or 100-fold while maintaining the salt concentration because at low concentration of D135, dimerization would be

slowed. Temperature was also decreased to 4˚C to minimize the disruption of dimer. (**Illustration 2.1A**) The quenched time points were loaded onto the gel within 1 minute. Indeed, the quench was successful as the dimer level at these time points was stable for at least 20 minutes (Data not shown). The rate of dimerization at 1 μM D135 was 0.93 min^{-1}, which was in a rough agreement with the rate measured by SAXS. At lower concentrations with 0.2 μM and 0.5 μM of D135, the dimerization rates were decreased and they showed a linear relationship rather than a quadratic relationship with D135 concentrations. (**Figure 2.2B and C**) (**Table 2.2**) This is rather surprising because for a one-step dimerization reaction, one can expect the rates would have quadratic relationship with the concentrations of the monomer. This result suggests the dimerization has a complex mechanism with more than one step.

I next examined the Mg^{2+} requirement for dimerization using SAXS. Previously, magnesium dependency on monomeric folding of D135 was studied using hydroxyl radical footprinting and ultracentrifugation.[5,6] These studies showed the tertiary folding and global compaction occur cooperatively at high magnesium concentration with K_{Mg}^{2+} = 15 mM ~ 47 mM and n_{Hill} = 1.5 ~ 2.3. It should be noted that under these previous structural studies the equilibrium was not reached as folding was only allowed for 10 to 15 minutes. The static SAXS measurements were performed after folding for an hour at 5 different Mg^{2+} concentrations. Guinier analysis showed that as Mg^{2+} concentration increased, R_g values decreased while I(0) values increased. (**Figure 2.3A and B**) Since I(0) value monitors the level of dimer, it is plausible that I(0) increases as dimer concentration increases. Although the overall size of D135 would increase after dimerization, R_g values decreased as D135 compaction overcame the increase in molecular weight. Overall, the plot of I(0) versus Mg^{2+} shows evidence for the high Mg^{2+} requirement for dimerization. If R_g values rather represented global compaction rather than dimerization, my result of K_{Mg}^{2+} = 13 mM and n_{Hill} = 2 agrees well with previous experiments for tertiary folding and global compaction. Therefore, this result suggests there is a correlation between folding and dimerization as dimerization has a similar dependency on Mg^{2+} concentration.

2.2 DIMERIZATION UNDER THE NEAR-PHYSIOLOGICAL CONDITION AND DISRUPTION OF DIMERS BY DEAD-BOX PROTEINS

An important question to ask was whether the dimerization might occur in a more physiologically relevant environment. I next examined dimerization process under the near-physiological condition (8 mM Mg^{2+}, 100 mM KCl, and 30˚C). Because other D135 folding studies from our lab were performed with inclusion of 10% of the Mss116 storage buffer (20 mM Tris pH 7.5, 500 mM KCl, 1 mM EDTA, 1 mM DTT, and 50% glycerol), my experiments also included 10% of the protein buffer. Unlike under the non-physiological condition with high Mg^{2+} concentration, time resolve SAXS shows I(0) and R_g values did not change much with a clear time-dependency for the first 5 minutes. (**Figure 2.4B and C**) There was also a minimal change during the observation time in the Kratky plots after initial, rapid electrostatic relaxation. (**Figure 2.4A**)

The dimerization process was further studied with the native gel assay for 3 hours. (**Illustration 2.1B**) As observed in the non-physiological condition, the concentration dependency was also observed. (**Figure 2.5A**) (**Table 2.3**) For high concentrations, there was an unresolved fast phase (> 3 min^{-1}). The level of dimer rather than the rate of the second phase had a concentration dependency, as the higher the concentration yielded a consistently higher fraction of the dimer. However, the data were difficult to be interpreted as a one-step dimerization reaction. If folding and dimerization are still correlated under this condition, it is plausible that dimerization would also follow a complicated kinetics with multiple phases as folding did.[10]

To examine several other elements that might affect dimerization, I first tested the change of the dimer level in the presence of the D135 substrate 17/7. It has been noted by Rueda and coworkers that binding of substrate stabilized the native state.[12] It is possible that the presence and the binding of the substrate stabilize either monomer or dimer and alter the dimerization kinetics. In order to study possible effects of the substrate, the dimerization kinetics was monitored by the native gel. The experiment showed the presence of 3-fold excess substrate

has little effect on the change of the dimer level. Also, there is little or no effect of the substrate on the dissociation of dimer at high magnesium. (**Figure 2.5B**) (**Table 2.3 and 2.4**) (**Illustration 2.1C**) A control experiment was performed to ensure that the substrates were bound to both monomer and dimer under the same experimental condition. Collectively, above results clearly state that the presence of substrate does not affect dimer level.

One obvious factor that may influence the level of dimerization is DEAD-box proteins. DEAD-box proteins are well-known structural disruption factors for structured RNAs and RNA-protein complexes.[16] DEAD-box proteins that I investigated are Mss116 and CYT19. To test if ATP-dependent unwinding activity of Mss116 actively disrupts the D135 dimer, D135 was pre-dimerized under the non-physiological condition. Then, salts and D135 were diluted to the near-physiological condition in the presence of Mss116 and ATP. There was a definite 10-fold increase in the rate of D135 dissociation, and this dissociation rate was correlated with the concentration of Mss116. It did not only increase the rate of dissociation, but also decreased the dimer fraction level by primarily disrupting the dimer. (**Figure 2.5C**) (**Table 2.4**) Spontaneous association of monomer was much slower than the structural disruption rate, so the apparent equilibrium of monomer and dimer seemed to be shifted toward monomer level. Another DEAD-box protein CYT-19 also could disrupt the dimer but in a less extent. When ATP was not added or ATP analogue adenosine 5'-(β,γ-imido)triphosphates (AMP-PNP) was added, the effect of DEAD-box proteins is negated. Surprisingly, the level of dimer started to increase after 30 minutes with the rate of 0.009 min^{-1}, which matched the rate of dimerization under the same condition. The simplest explanation is that D135 spontaneously started to dimerize again after possible protein death and/or ATP depletion. Together, this result provides direct evidence that ATP-dependent unwinding activity of DEAD-box proteins can facilitate the disruption of D135 dimers.

Next, I investigated how unwinding activity affected the dimerization process that started from the unfolded monomer under the near-physiological condition. The dimerization reaction with Mss116 in the absence of ATP had a minimal effect on the dimerization process. However,

when Mss116 was added to the reaction in the presence of ATP, the reaction became more complicated. For the first 1 hour, there was an impediment in the dimerization process. After an hour, it seems spontaneous dimerization was resumed, which might be caused by ATP depletion or protein death as observed in the dimer disruption experiment with a high Mss116 concentration. Particularly for the reaction with the high concentration of Mss116 (0.8 μM), it was first disrupted for the first 30 minutes, and dimerization proceeded more rapidly than the reaction without the protein. (**Figure 2.5D**) It is possible that correctly folded monomer by ATP-dependent Mss116 activity may be prone to dimerize faster than unfolded monomer. However, the experiment was only performed once, so a further investigation is necessary to make a confident conclusion. Nevertheless, the initial disruption of dimerization by Mss116 is fully consistent with the model where Mss116 actively disrupts dimers from the above dimer dissociation experiments.

2.3 D135 DIMERIZATION DOES NOT AFFECT ITS CATALYSIS

To examine the implication of dimerization for the function of D135 and possibly of the group II intron, the relationship between the dimerization level and the catalysis was investigated. To study this relationship, the multiple turnover cleavage assay at the non-physiological condition was used, as this method is a valuable tool for probing the appearance of catalytically active states.[17] The hypothesis is if the dimer is the only catalytically active species, the rate of cleavage will be dependent on D135 concentration when dimerization is slower than catalysis and folding.

To study this, I examined the kinetics of catalytic onset when starting from unfolded ribozyme. Unfolded D135 at three different concentrations, spanning from 0.5 μM to 2 μM, was added to the 3-fold excess substrate and folding buffer with Mg^{2+} and K^{+} simultaneously, and the rate of product formation was monitored. A parallel experiment with prefolded and dimerized D135 at the same condition was initiated with the addition of the substrate. The equivalence

product relative to ribozyme was plotted over time, and the data were fitted into the burst equation. (See Chapter 3.4) The rate of the burst represents the initial rate of cleavage in a single-turnover, and the subsequent turnover is rate-limited by product release. All three concentrations of D135 yielded the similar cleavage rate of 1.3 min^{-1} for prefolded controls and 0.6 min^{-1} for continuous folding assays, with comparable amplitudes without a clear concentration dependency. (**Figure 2.6A**) (**Table 2.5**) This result is deviating from the previously reported values by Pyle and colleagues, whose rate of cleavage was reported as 3 min^{-1} and rate of folding as 1 min^{-1}.[5] Also, there was a concentration determination issue that was possibly due to substrate degradation as the amplitude of the burst was higher than 1. Regardless, a conclusion that D135 dimer is most likely active as the rate of dimerization is similar or faster than the rate of the catalytic onset at the tested concentrations of D135. However, the cleavage was not rate limited by the dimerization and the rate of dimerization was not slower than the catalysis, so it was not clear whether the monomer form of D135 is active.

Next, I wanted to test whether D135 monomer is catalytically active. To assure that D135 monomer is active, I compared the rate of dimerization and the rate of native folding under conditions where the rate of native folding is faster than dimerization. Since it is not straightforward to perform catalytic activity assays at such a low concentration of D135 as binding of substrate may be slowed and become the rate-limiting step. I also compared the folding started from monomer and the pre-folded dimer so that it can be a further support if the rate of catalysis is the same for both dimeric and monomeric D135. To do this, the low concentration of unfolded or prefolded D135 was incubated at the near-physiological condition so that both pre-dimerized and monomeric unfolded D135 are in the same condition. The substrate was allowed to be bound under this condition as well. Then, D135 jumped to the non-physiological condition where the catalysis was favored. (**Illustration 2.1D**) For two different concentrations of unfolded and dimerized D135 yielded the same rate of catalysis with the average at 0.75 min^{-1}. (**Figure 2.6C**) The rate of dimerization under this condition was determined to be 0.19 min^{-1} for 0.125 μM D135 and 0.33 min^{-1} for 0.25 μM D135. (**Figure 2.6B**)

(**Table 2.6**) Thus, the rate of dimerization is sufficiently slower than the catalysis, and it can be evidence that monomers are catalytically active. Overall, the dimerization process does not affect the catalytic activity of D135 ribozyme.

2.4 TIME-RESOLVED SHAPE FOOTPRINTING TO PROBE THE DIMERIZATION INTERFACE

Next, I attempted to probe the possible regions that mediate dimerization. The simplest approach is to explore the structural difference between monomer and dimer. The monomer would be favored in a concentration lower than K_d. However, it is not very straightforward to perform footprinting experiments that employ primer extension because a certain amount of RNA is required. Therefore, I decided to use the time-resolved footprinting approach to monitor the progress of dimerization under the non-physiological condition. From the course of time, unfolded monomers are converted to folded dimers. There would be intra-molecular changes that are dictated by the tertiary folding of the ribozyme, as well as inter-molecular changes that occur during dimerization process. At the concentration of D135 (0.2 μM), the tertiary folding process occurs at the rate of ~1 min^{-1} in the non-physiological condition[5, 10, 12] while the dimerization occurs at the rate of 0.4 min^{-1}. The difference in the rates is not decisively different, but if there is a structural change that matches the rate of dimerization, I would be able to make an educated guess on possible dimerization interface.

The footprinting method that I applied to tackle this goal is the selective 2'-hydroxyl acylation analyzed by primer extension (SHAPE) footprinting. This method utilizes an acylation reagent that selectively modifies flexible nucleotides on its 2' hydroxyl group, while base-paired nucleotides remain unreactive toward the reagent. The reagent used in this study was the fast-acting SHAPE reagent, benzoyl cyanide. It has been shown that benzoyl cyanide can react with the 2' hydroxyl group of ribose in a millisecond range.[18] One useful feature of this SHAPE reagent is that it also react with water in the same time-scale, so no additional quench step is necessary for time-resolved approach.

Using this method, the dimerization process at non-physiological condition was monitored for 19 minutes. There are several regions with differential reactivity over course of time, and most of them became less reactive (more protected) over the course of time. (**Figure 2.7**) (**Table 2.7**) These regions had the rate of protection varying from 0.2 min^{-1} to 7 min^{-1} and were mostly corresponding to the regions of previously identified tertiary contacts. One surprising region was the DIV stem-loop, which folded at the similar time scale with other tertiary contact regions. The two exon-binding sequences became more reactive with the similar rate constants as well. As I expected and realized, the biggest caveat in this method to locate dimerization region is that it is not very straightforward to distinguish folding and dimerization as the rates are not very discernible. Regardless, the footprinting result showed that native tertiary contacts were still forming even in the dimerizing condition.

2.5 ARTIFICIAL 3' TAIL MEDIATES THE DIMERIZATION

Next, I explored possible dimerization interfaces. One possibility that I noticed is that there is an artificially added region by Pyle and colleagues, who designed the ribozyme: 3' tail with 35 nucleotides. This region is basically the multi-cloning site of pUC19 plasmid, and it was initially included in the ribozyme for the primer-extension purpose. Since this region contains many palindromic sequences for restriction enzyme recognition sites, it is possible that this region could mediate dimerization. Therefore, I hypothesized that dimerization could be abolished when this region is deleted. I made a new construct of D135 with a shortened 3' tail of 7 nucleotides.

Dimerization of D135 without the long 3' tail was tested with the native gel mobility shift assay at the non-physiological condition. Various concentrations of this D135 construct from 2 nM to 500 nM were allowed to be dimerized for 1 hour. Even at the highest concentration, no visible second band was observed in the native gel. Dimerization was effectively abolished with deletion of this tail, which provides strong support that the dimerization was mediated by the

base-pairing of this long artificial 3' tail. (**Figure 2.8**) This finding was consistent with the discovery that the DEAD-box proteins could disrupt dimerization by presumably unwinding the base-pairings. Because of a technical difficulty, RNAs were body-labeled in the experiment, and the positive control experiment by D135 with the 3'tail was performed in the same manner. It should be noted that the dimer dissociation constant of D135 with the 3'tail was at least 7-fold higher than the previous measurements possibly due to differences in the RNA preparations, but a concise explanation of this discrepancy was not identified.

2.6 DISCUSSION

The SAXS data and native gel experiments in this study collectively provided evidence that the D135 ribozyme, which was used over a decade by several research groups, dimerizes under both non-physiological and near-physiological conditions. Dimerization of D135 was first observed by SAXS experiments during global structural study of D135, which was partially successful to demonstrate that there is a rapid compaction event during folding under the non-physiological condition. The presence of stable dimerization was further supported by the independent analytical ultracentrifugation work that was done previously.[6] As the Mg^{2+} titration SAXS experiments show, this process requires high Mg^{2+} with K_{Mg}^{2+} = 13 mM. Also, the kinetics of dimerization is dependent on the concentration of the ribozyme. As the reaction order for the kinetics of dimerization is not a second-order process with respect to ribozyme concentration, dimerization is rather a multi-step and complicated process than a simple one-step process.

The important question that I must ask after its characterization was if this dimerization is biologically important. Time-resolved SHAPE footprinting analysis shows that most of the native contacts are formed in dimers, and there were no other obvious regions that may involve in dimerization. The region uninvestigated through footprinting includes the 3' end of D135 where the primer for reverse transcription binds. As I expected, the deletion of the artificially

added 3’ tail strongly reduced the dimerization process. This suggests that this dimerization is merely an artifact without any physiological significance. The conclusion that ATP dependent activity of DEAD-box proteins disrupts dimerization is fully consistent with the fact that dimerization is mediated by simple base-pairing in the complementary 3’ tail.

Although the dimerization is not physiologically significant, it is still an important finding that a researcher must be aware of when studying this ribozyme. Most notably, during global analysis of this ribozyme using SAXS, it will become more straightforward to relate the size and shape change to the folding process without dimerization when the 3’ tail-less D135 is used. Also, I could not find any control experiment that was done to ensure this 3’ tail region does not interfere with folding. The observation that this ribozyme has a similar magnesium requirement as folding suggests that there must be some correlation between folding and dimerization. Therefore, it is important to determine whether this region interferes with ribozyme folding.

	Amplitude (Å)	k (min^{-1})
Avg R_g ± Std Dev	6.7 ± 1.7	0.59 ± 0.01
Avg I(0) ± Std Dev	0.003 ± 0.001	0.6 ± 0.4

Table 2.1 Guinier analysis for time-resolved SAXS

[D135] μM	Amplitude	k (min^{-1})
0.2	0.65	0.40
0.5	0.71	0.63
1.0	0.77	0.93

Table 2.2 Dimerization observed by native gel at the non-physiological condition

	First phase		Second phase	
Condition	Amplitude	k (min^{-1})	Amplitude	k (min^{-1})
0.2 μM D135	0.08	3.5	0.46	0.009
0.5 μM D135	0.18	3.9	0.33	0.02
0.8 μM D135	0.20	2.3	0.39	0.02
0.5μM D135 + 1.5 μM Substrate	0.20	1.9	0.41	0.009
0.5 μM D135 + 0.5 μM Mss116, no ATP	0.28	3.9	0.38	0.01
0.5 μM D135 + 0.2 μM Mss116 + ATP	N/A			
0.5 μM D135 + 0.5 μM Mss116 + ATP	N/A			
0.5 μM D135 + 0.8 μM Mss116 + ATP	N/A			

Table 2.3 Dimerization observed by native gel at the near-physiological condition

0.5 μM D135	Amplitude	k (min^{-1})
D135 only	0.19	0.0082
+ 1.5 μM Substrate	0.26	0.0088
+ 0.5 μM Mss116, no ATP	0.25	0.0067
+ 0.5 μM Mss116, AMPPNP	0.25	0.0077
+ 0.2 μM Mss116, ATP	0.54	0.083
+ 0.5 μM Mss116, ATP	0.68	0.094
+ 0.8 μM Mss116, ATP	0.85	0.0197
+ 0.5 μM CYT19 ATP	0.36	0.06

Table 2.4 Dimer dissociation at the near-physiological condition

	Prefolded Control			Continuous Folding Assay		
[D135]; [Substrate]	Burst amplitude	Burst rate (min^{-1})	Rate of linear phase (min^{-1})	Burst amplitude	Burst rate (min^{-1})	Rate of linear phase (min^{-1})
0.5 μM; 1.5 μM	1.57	1.47	0.032	1.79	0.59	0.021
1.0 μM; 3.0 μM	1.57	1.24	0.026	1.64	0.64	0.014
2.0 μM; 6.0 μM	1.73	1.23	0.017	1.93	0.55	0.018

Table 2.5 Continuous folding assay and prefolded D135 control at various [D135]

	Dimerization			Dimer Dissociation		
[D135]	Amplitude	k (min^{-1})	Initial point	Amplitude	k (min^{-1})	Initial point
0.125 μM	0.34	0.33	0.14	0.18	0.03	0.58
0.25 μM	0.37	0.19	0.08	0.20	0.03	0.66
	Catalysis (Starting with Monomer)			Catalysis (Starting with Dimer)		
[D135]	Burst amplitude	Burst rate (min^{-1})	Rate of linear phase (min^{-1})	Burst amplitude	Burst rate (min^{-1})	Rate of linear phase (min^{-1})
0.125 μM	2.4	0.79	0.018	2.4	0.87	0.016
0.25 μM	2.3	0.70	0.020	2.3	0.83	0.016

Table 2.6 Comparison between dimerization rate and catalysis rate

Less Reactive Over Time		More Reactive Over Time	
Tertiary contacts or grouped nucleotides	k (min^{-1})	Tertiary contacts or grouped nucleotides	k (min^{-1})
α (60~65)	2.5	Loop (158~161)	2.6
θ (98~101)	1.1	EBS2 (238~243)	1.0
λ (116)	0.78	Loop (289~292)	2.7
ε’ (117~118)	1.4	EBS1 (329-336)	1.8
ς (197~201)	7		
μ (469-470)	0.24		
DIV (525, 527, 531, 528, 542,546)	2.2		
ς’ (562~565)	0.7		

Table 2.7 Rate constants calculated from time-resolved SHAPE footprinting

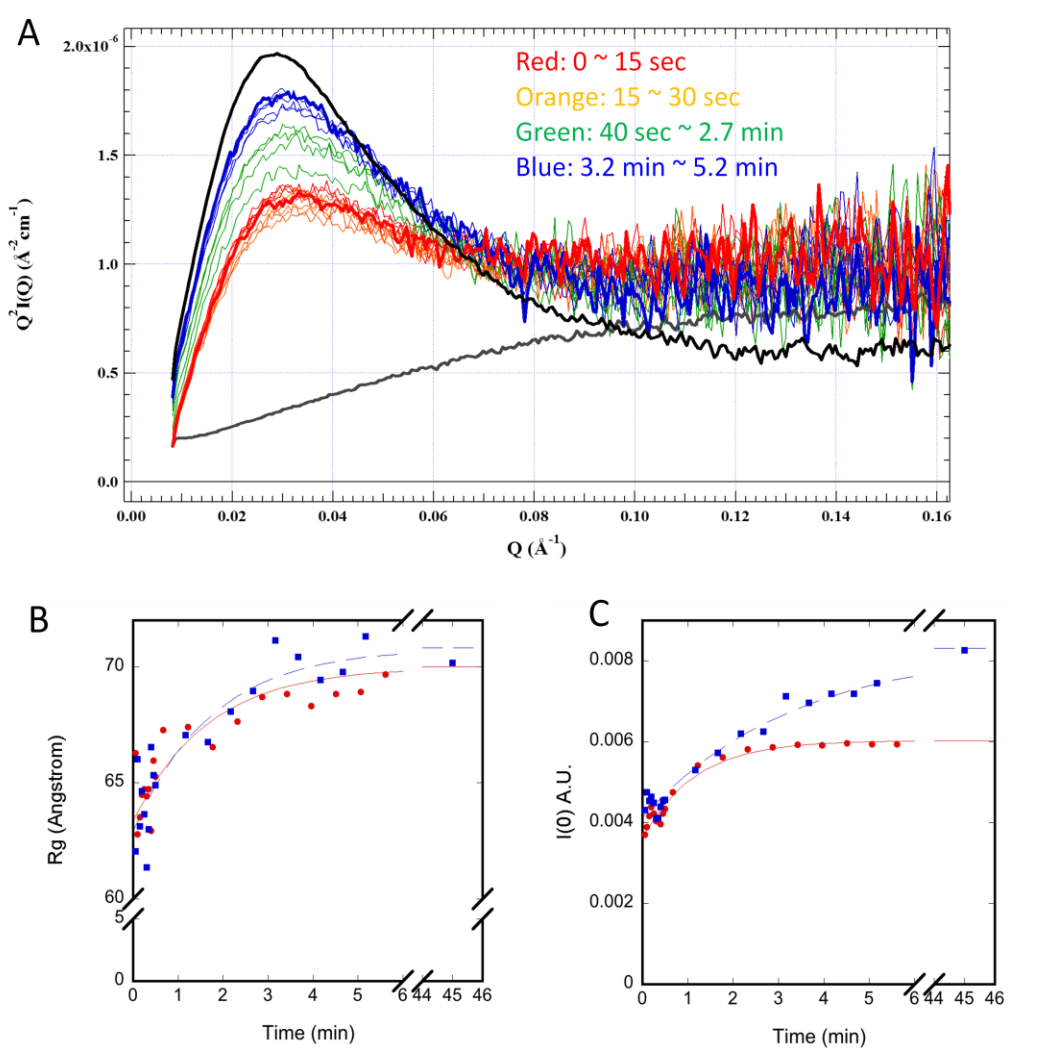

Figure 2.1 Time resolved SAXS at the non-physiological condition

(A) Kratky plots of time-resolved SAXS data and static measurements are shown. Measurements were started to be taken <3 seconds after mixing the folding buffer and heat-denatured D135 ribozyme. 1 μM of D135 were used in these experiments. The gray curve and the black curve represent the static measurement of unfolded D135 and fully folded D135, respectively. The curves are grouped in colors based on their time points: red lines (0~15 seconds), orange lines (15~30 seconds), green lines (40 seconds~2.7 minutes), and blue lines (3.2~5.2 minutes). (B, C) The change in R_g and I(0) values determined by Guinier approximation is plotted against time. Blue and red curves are the duplicate of the same experiment except the measurements were taken at different beam-times and with different RNA preps. The error possibly came from differences in the quality of RNA preparation.

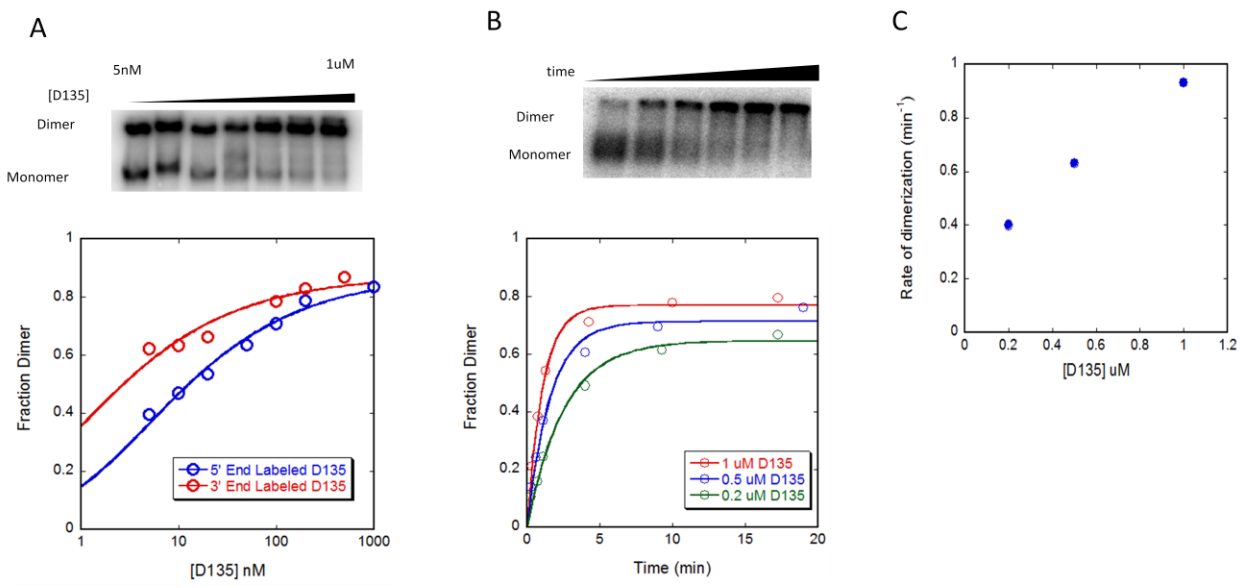

Figure 2.2 Observation of dimerization by native gel at the non-physiological condition

(A) The native gel image of the electrophoretic mobility shift assay for dimerization equilibrium is shown. Fractions of dimer at various D135 concentrations are plotted. (B) The native gel image of time-resolved dimerization experiment is shown. Progress of increase in dimer fraction is plotted. Three different concentrations of D135 were used in the experiment. (C) The rate of dimerization at each D135 concentration is plotted.

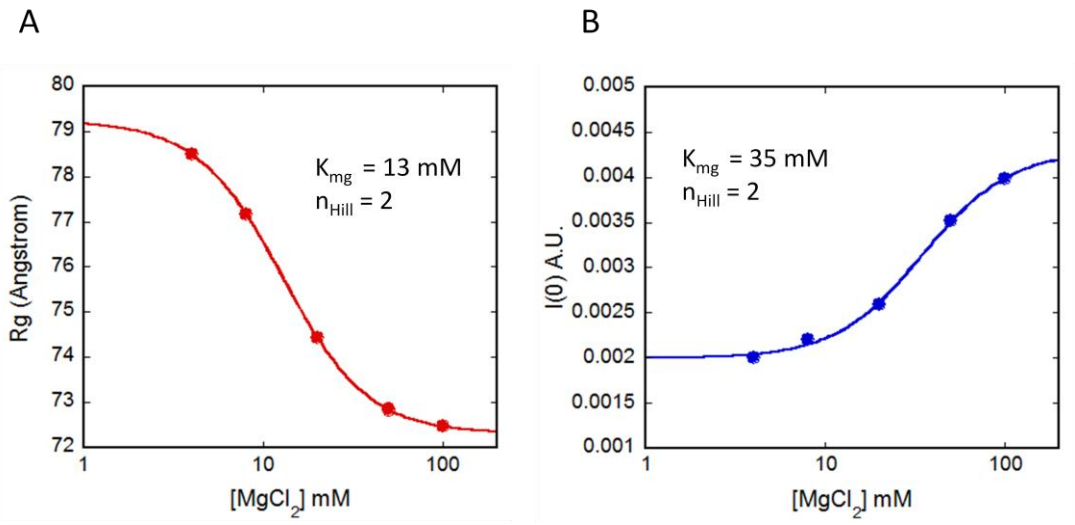

Figure 2.3 Magnesium requirements for ribozyme compaction and dimerization.

(A, B) Static measurements of R_g values and I(0) values at various magnesium concentration were determined by Guinier analysis. The magnesium concentration dependency curve of R_g and I(0) were plotted and fitted with Hills equation.

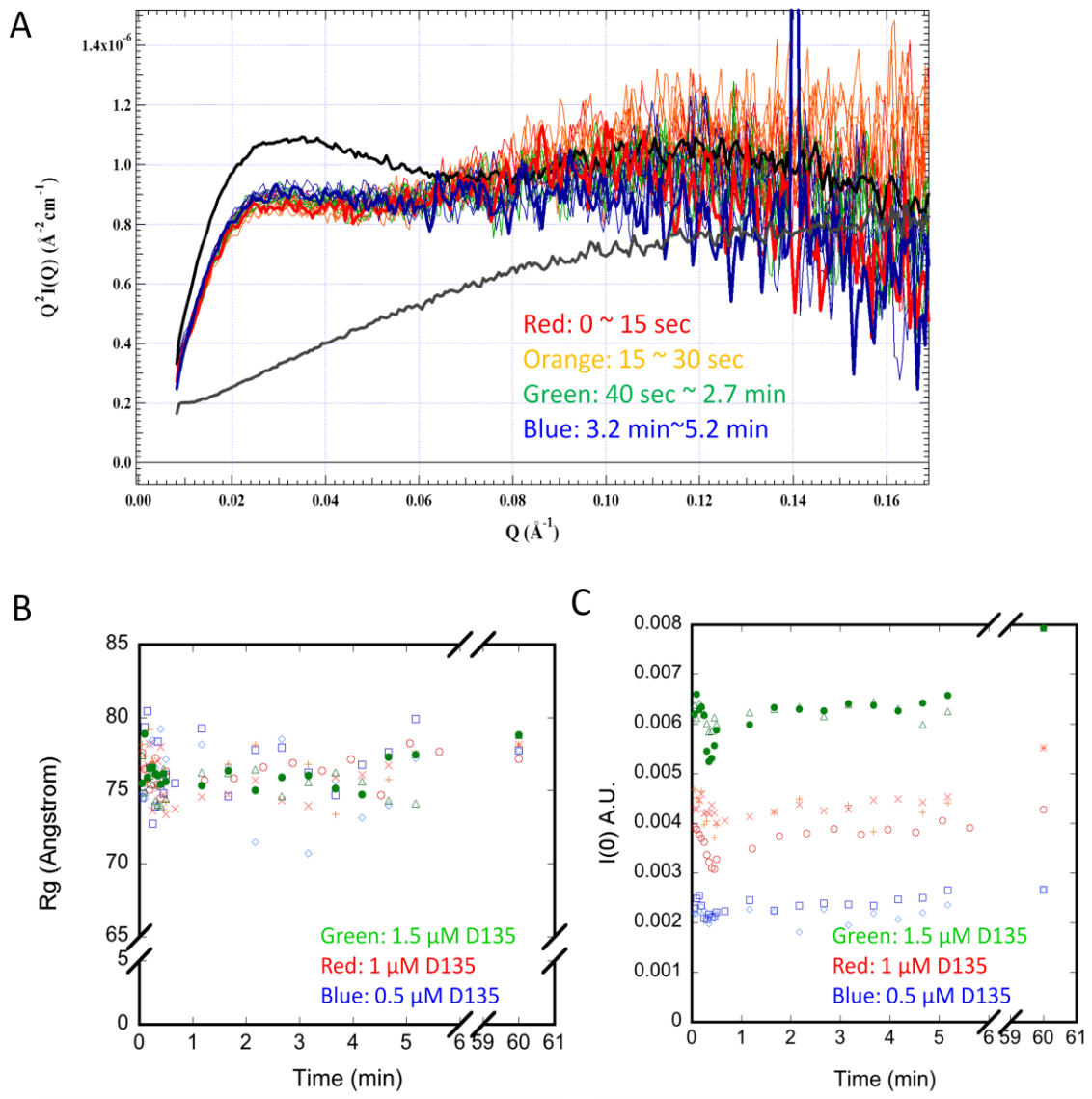

Figure 2.4 Time resolved SAXS at the near-physiological condition

(A) Kratky plots of time-resolved SAXS data and static measurements are shown. Measurements were started to be taken < 3 seconds after the folding buffer and heat-denatured D135 ribozyme are mixed. The concentration of D135 after mixing was 1uM. The gray curve and the black curve represent the static measurement of unfolded D135 and fully folded D135, respectively. The curves are grouped in colors based on their time points: red lines (0~15 seconds), orange lines (15~30 seconds), green lines (40 seconds ~ 2.7 minutes), and blue lines (3.2 ~ 5.2 minutes). (B, C) The change in R_g and I(0) values determined by Guinier approximation is plotted against time. Three different concentrations of D135 were used in the experiment, either in duplicate or triplicate.

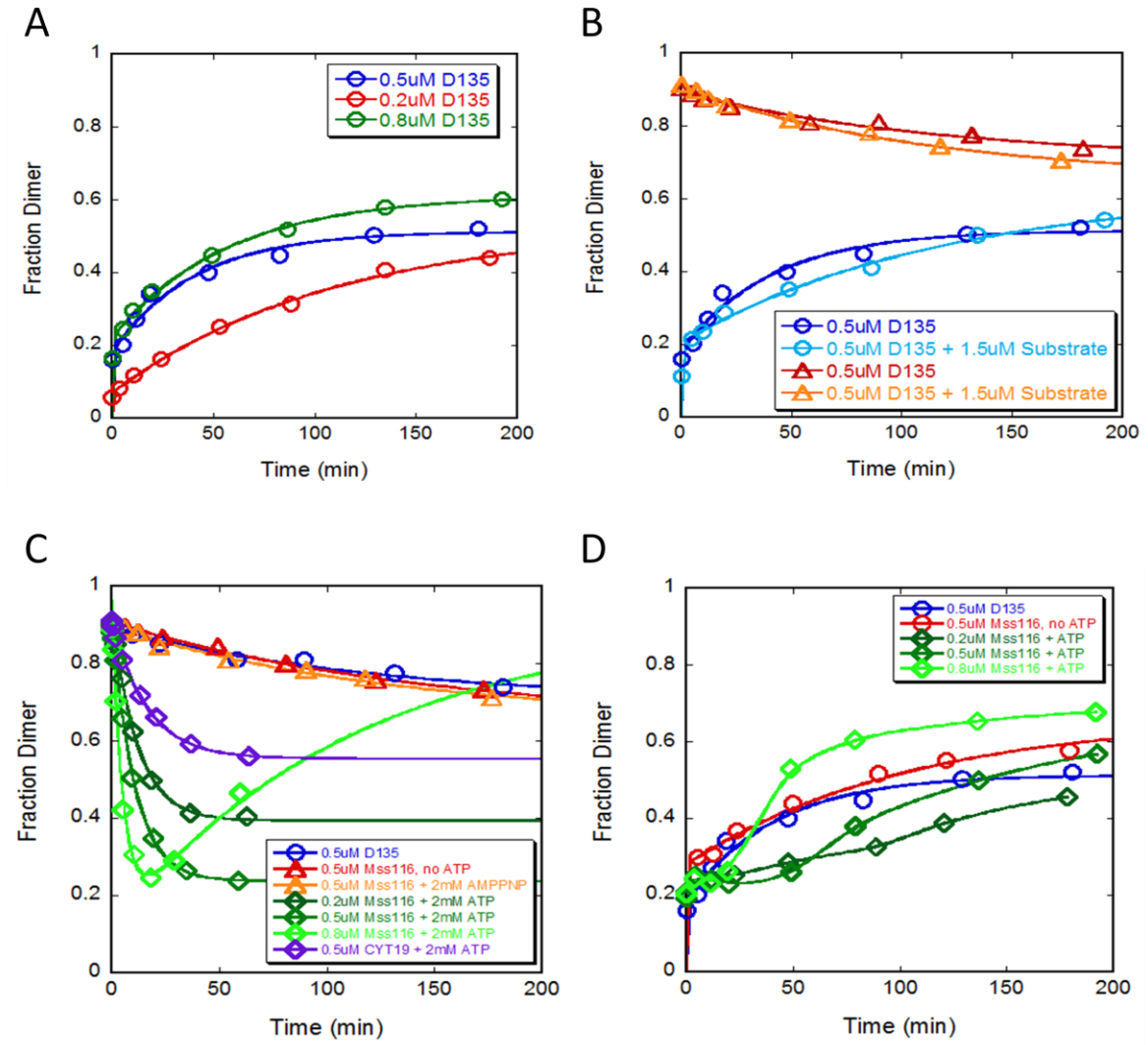

Figure 2.5 Dimerization and dissociation of dimers at the near-physiological condition and active disruption of dimers by DEAD-box proteins.

(A) Progress curves for D135 dimerization at the near-physiological condition are shown. Three different concentrations of D135 were used. (B) D135 dimerization and dimer dissociation kinetics were measured in the presence or absence of 3-fold excess of the substrate relative to D135 concentration. The upper curves represent the dimer dissociation experiments, and the lower curves represent dimerization experiment. (C) Progress curves for dimerization in the presence or absence of DEAD-box proteins with or without ATP are shown. (D) It shows the progress curves for dimer dissociation in the presence or absence of DEAD-box proteins with or without ATP or ATP analog.

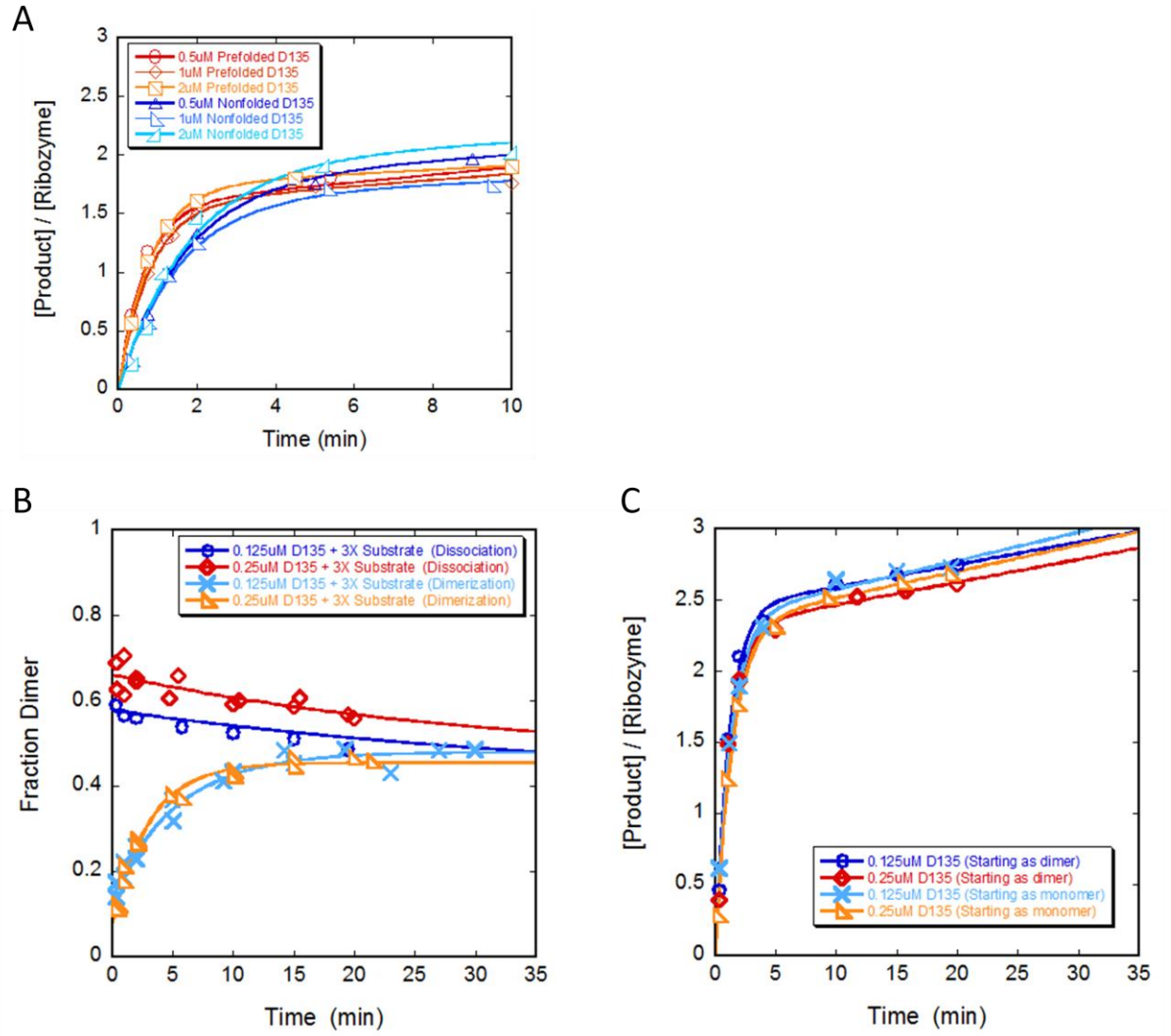

Figure 2.6 Effect of dimerization on catalysis

(A) Multiple turnover substrate cleavages by pre-folded or not pre-folded D135 at various concentrations were monitored. Red and orange curves are progress curve for the prefolded controls, and the blue and light-blue curves are continuous folding assays. (B) Level of dimers was monitored after the sample was added to non-physiological condition.

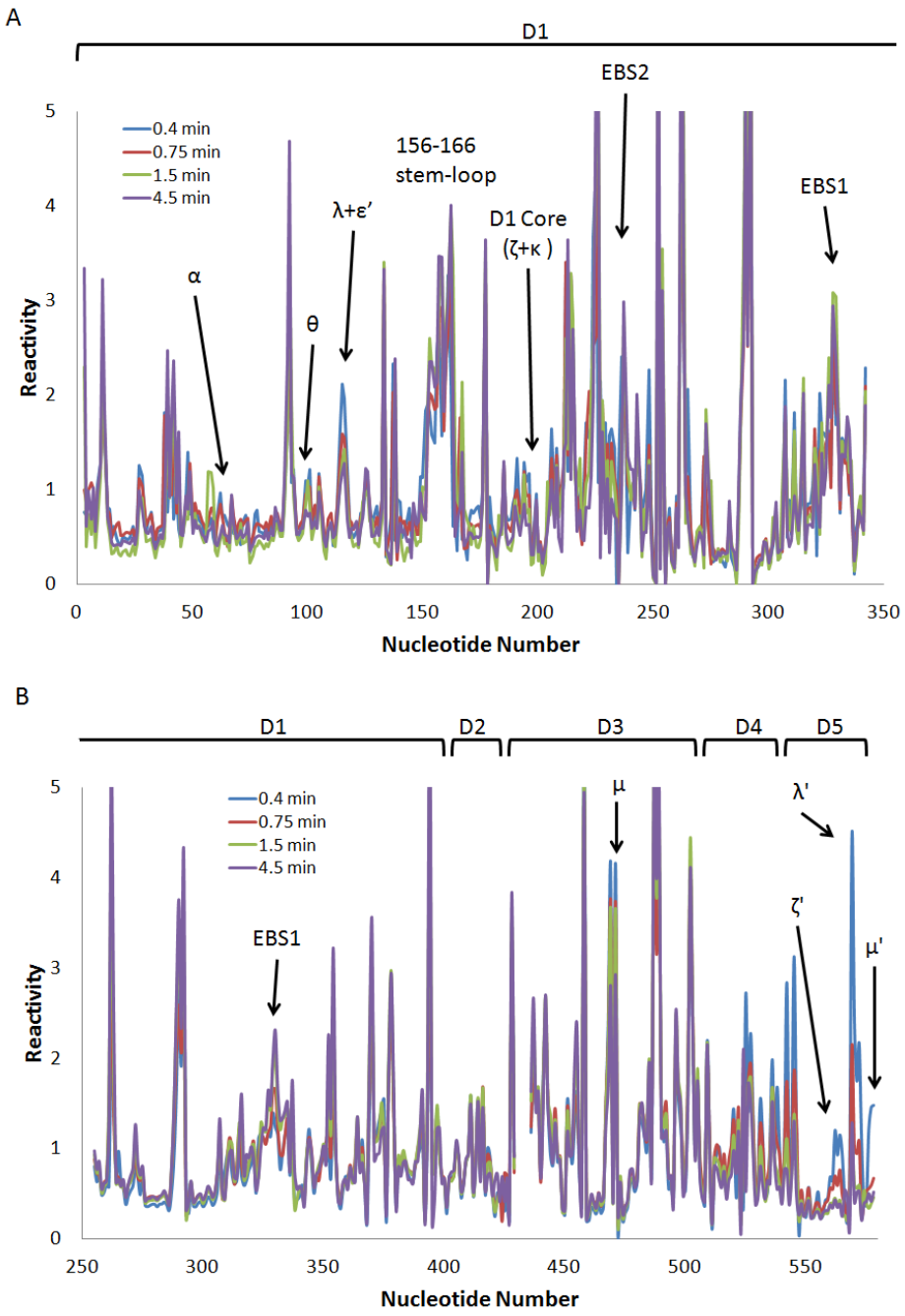

Figure 2.7 Time-resolved SHAPE footprinting

The first 4 time points, where reactivity differences were prominent, are shown as a plot of normalized reactivity at each nucleotide residue number. (A) Reactivity profile for nucleotides from 2 to 342, which were mapped by a primer that binds nucleotides from 375 to 405 of D135. (B) Reactivity profile for nucleotides from 255 to 578, which were mapped by a primer that binds nucleotides from 593 to 616. The tertiary contacts and regions that had time-dependent changes in reactivity are labeled on the graph.

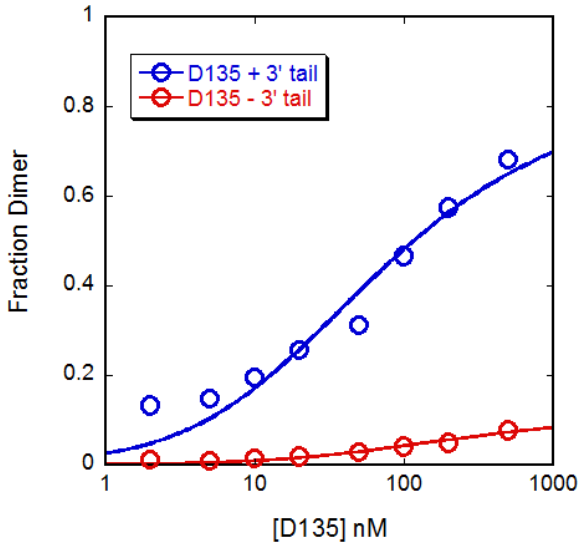

Figure 2.8 The 3’-tail mediates dimerization

Various concentrations of D135 ribozymes with and without 3’-tail were folded under the non-physiological condition. The fractions of dimers were plotted against D135 concentrations.

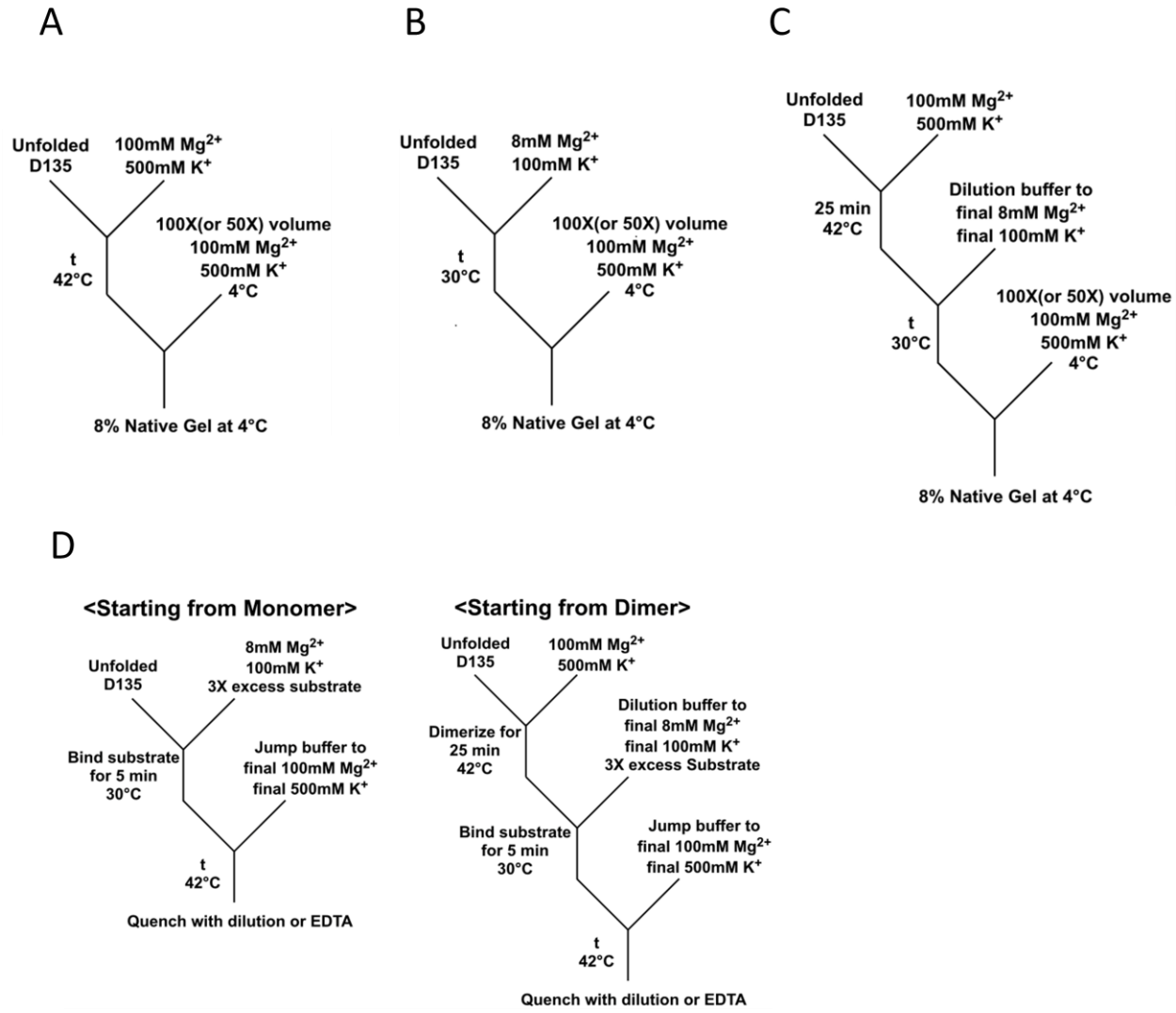

Illustration 2.1 Reaction schemes

Chapter 3: Materials and methods

3.1 RNA PREPARATION

D135 ribozyme and D135 without the 3' tail were transcribed by the T7 RNA polymerase *in vitro* transcription system with HindIII-digested plasmid and BamHI-digested plasmid as the templates, respectively. Transcribed RNA was purified with ethanol precipitation and Qiagen RNeasy column. The D135 substrate, 17/7, was purchased from Dharmacon. D135 RNA is 5' end labeled, 3' end labeled, or body labeled. For 5' end labeling, transcribed D135 was first phosphatized by Shrimp Alkaline Phosphatase (NEB), and then phosphorylated with [γ -^{32}P] ATP (Perkin Elmer) by T4 polynucleotide kinase (NEB). For 3' end labeling, a template oligonucleotide complementary to 3' end of D135 was used for addition of [α-^{32}P] dATP (Perkin Elmer) by Klenow fragment (NEB), as described previously.[19] For body labeling, RNA was transcribed in the presence of [α-^{32}P] UTP (Perkin Elmer). The labeled RNA was then gel-purified with 8% non-denaturing polyacrylamide gel. Substrate 17/7 was 5' end labeled as described above. Concentrations of D135 and its substrate were determined by the absorbance at 260 nm with extinction coefficients of 5.86 x 10^6 M^{-1} cm^{-1} and 2.36 x 10^5 M^{-1} cm^{-1}, respectively.

3.2 PROTEIN PURIFICATION

Mss116 and CYT19 were purified as described[20], but with a slight modification. Instead of Ceramic Hydroxyapatite column (Biorad), Heparin column (GE) was used. Purified protein was then dialyzed with the protein buffer composed of 20 mM Tris pH 7.5, 500 mM KCl, 1 mM EDTA, 1 mM DTT, and 50% glycerol, and stored at -80°C until it was used in experiments.

3.2 EQUILIBRIUM AND TIME-RESOLVED SAXS MEASUREMENT

SAXS measurements were taken on beamline 12-ID-C at Argonne National Laboratory. For static non-physiological condition measurements, D135 in MOPS buffer was first denatured at 95˚C and added to folding buffer to final concentration of 1 μM D135, 50 mM NaMOPS at pH

7.0, 100 mM $MgCl_2$, and 500 mM KCl. Folding was proceeded for 1 hour, and was put on ice until the static shots were taken. For near-physiological condition measurements, the experiment was done with the same manner as above with final concentrations of 1 μM D135, 50 mM NaMOPS at pH 7.0, 8 mM $MgCl_2$, and 100 mM KCl, 5% glycerol. For magnesium titration experiment, the condition was essentially the same as the near-physiological condition except magnesium concentration. The samples were injected to the observation cell by the stop-flow mixer (Hamilton Microlab 500). Guinier analysis was performed by Igor Pro after averaging and buffer subtraction. The data of R_g and I(0) at various Mg^{2+} concentrations were plotted and fitted to a Hill equation:

$$R_g or\ I(0) = \frac{[Mg^{2+}]^{n_{Hill}}}{K_{Mg^{2+}}{}^{n_{Hill}} + [Mg^{2+}]^{n_{Hill}}}$$

where $K_{Mg}{}^{2+}$ represents the magnesium concentration at which half of the ribozyme is folded and dimerized, and n_{Hill} represents the measure of cooperativity.

For time-resolved experiments at both conditions, folding was initiated by rapidly mixing the unfolded D135 solution and the folding buffer in an equal volume while the temperature was controlled either at 42°C or 30°C by a thermoelectric cooler. First, ten shots were taken with 3 second interval and the next ten shots were taken with 13-second interval. SAXS data were analyzed after averaging and buffer subtraction, and Guinier analysis and Kratky plot analysis were performed by Igor Pro (WaveMetrics). The progress curve of R_g and I(0) value changes was fitted with single-exponential equation:

$$R_g or\ I(0) = A * (1 - e^{-k*t}) + initial\ point$$

where k represents the rate of dimerization, and A represents the amplitude of change.

3.3 NATIVE GEL ELECTROPHORETIC MOBILITY SHIFT ASSAY FOR MONITORING DIMERIZATION EQUILIBRIUM AND KINETICS

Dimerization equilibrium was measured after RNA was folded for 1 hour at the non-physiological condition (50 mM NaMOPS at pH 7.0, 100 mM $MgCl_2$, and 500 mM KCl) and

for the near-physiological condition (50 mM NaMOPS at pH 7.0, 8 mM $MgCl_2$, and 100 mM KCl, 5% glycerol) with variable D135 concentrations, ranging from 5 nM to 1 μM with a trace amount of 5'- or 3'- labeled D135. RNA was denatured before the folding step. RNA is then mixed with an equal volume of dye solution while maintaining the magnesium concentration. Monomer and dimer are separated with 8% native PAGE (30 mM Tris, 60 mM Mes, 0.1 mM EDTA, 10 mM MgCl2, and 300 mM KCl at 4°C) for 3 hours at 280 V and quantified by PhosphorImager.

The equilibrium between monomer and dimer is described by the following equation:

$$2\,Monomer \leftrightarrow Dimer$$

Thus, the dissociation constant for dimer is given by the following equation:

$$K_d = \frac{[Monomer]^2}{[Dimer]} = \frac{([D135]_{total} - 2 * [Dimer])^2}{[Dimer]}$$

By rearranging the above equation and solving for dimer concentration, the following equation is deduced:

$$\frac{[Dimer]}{[D135]_{total}} = \frac{K_d + 4 * [D135]_{total} - \sqrt{K_d * (K_d + 8 * [D135]_{total}}}{8 * [D135]_{total}} * A$$

where K_d represents the dimer dissociation constant and A represents the maximum amount of dimer that can be achieved. The plot of the fractions of dimer against D135 concentrations was fitted to the above quadratic equation.

The kinetics of dimerization at both conditions was measured as heat denatured RNA in MOPS buffer was added to the folding buffer, and each time point was quenched by diluting the RNA by 50- or 100-fold with the buffer for the non-physiological condition where dimer was shown to be stable. The quenched time points were loaded within two minutes to separate monomers and dimers. Dimerization in the presence of substrate and dimerization in the presence of DEAD-box proteins were performed exactly the same as the near-physiological condition except substrates, proteins, and/or ATP or AMP-PNP were added. The amount of dimer and monomer were quantified as described above. The plots of dimer fraction and time were fitted to a single-exponential equation:

$$Fraction\ Dimer = A * (1 - e^{-k*t})$$

where A represents the amplitude of change and k represents the rate of dimerization. In some reactions where multiple phases were apparent, the plots were fitted to a double exponential equation:

$$Fraction\ Dimer = A_1 * (1 - e^{-k_1 t}) + A_2 * (1 - e^{-k_2 t})$$

where A_1 and A_2 represent the amplitudes of first and second phases, and k_1 and k_2 represent the rates of first and second phases, respectively.

For dimer dissociation reactions, D135 was first dimerized in the non-physiological condition at a high D135 concentration, and then ribozyme and ions were diluted simultaneously to the near-physiological condition. Proteins and substrates were present in the dilution buffer if indicated. At various time points after dilution, aliquots of reaction were quenched by diluting 50-fold in buffer that matches the non-physiological condition. The amounts of dimer and monomer were quantified as described above. The plots of dimer fraction and time were fitted by the single exponential decay equation:

$$Fraction\ Dimer = A * e^{-k*t}$$

where A represents the amplitude of change and k represents the rate of decay.

3.4 MULTIPLE TURNOVER CATALYTIC ACTIVITY AND FOLDING ASSAY

The multiple-turnover catalytic activity assay was done essentially as described.[5] For the prefolded control, D135 at various concentrations, ranging from 0.5 μM to 2 μM, was denatured at 90˚C for 1 minute in EPPS buffer (pH 8), and the 100 mM $MgCl_2$ and 500 mM KCl were added and D135 was folded at 42˚C for 20 minutes. Catalysis was initiated as 5' end labeled substrate was added in 3-fold excess to ribozyme while maintaining salt concentration. For the continuous folding assay where folding and catalysis were concerted, 100 mM $MgCl_2$ and 500 mM KCl were added to the heat-denatured D135 simultaneously with 3-fold excess substrate. For both cases, aliquots of reaction were quenched at various time points after initiation by

addition of two fold volume of 100 mM EDTA and formamide. The 5' end labeled substrate and the 5' product were separated by 7 M urea denaturing 20% polyacrylamide gel at 16 W for 1 hour, and quantified by PhosphorImager. The plot of equivalent product with respect to amount of ribozyme was fitted with the burst equation:

$$\frac{[Product]}{[Ribozyme]} = A * (1 - e^{-k_1 t}) + k_2 t$$

where the burst rate (k_1) refers to first-turnover cleavage rate, which is rate-limited by the folding in continuous folding assay, and the linear rate (k_2) is rate-limited by the slow product release. Amplitude represents the fraction of the active ribozyme.

3.5 BENZOYL CYANIDE SHAPE FOOTPRINTING

Benzoyl cyanide (BzCN) was used as a 2'-OH alkylating reagent as it is the fast-acting one that reacts in a millisecond time scale. Time resolved SHAPE footprinting was performed as described in the previously published protocol with appropriate modifications.[18] D135 ribozyme at 0.2 μM was first denatured at 90˚C for 1 minute in MOPS (pH 7), and folding and dimerization of unfolded monomeric D135 were initiated with the addition of 100 mM $MgCl_2$ and 500 mM KCl at 42˚C. At various time points, 25 μl of the reaction was added to 2.5 μl of 40mM BzCN in dimethyl sulfoxide (DMSO) and mixed by pipetting immediately. For a no-footprinting control, the same amount of RNA was added to 2.5 μl of DMSO.

Footprinted ribozyme samples were then ethanol precipitated, washed with 70% ethanol, and resuspended in 10 μl of annealing buffer (50 mM Tris pH 8.3, 60 mM KCl, 10 mM DTT). Primer extension was performed as described.[21] Two cy5-labeled DNA primers (IDT) complementary to D135 residue numbers from 375 to 405 and from 593 to 616 were allowed to bind by denaturing at 85˚C and slowly cooling down to 25˚C. Primer extension buffer that contained a certain amounts of magnesium, dNTPs, and Superscript III reverse transcriptase (Invitrogen) for an optimal reaction was added to primer-RNA complex. Reverse transcription was performed at 55˚C for 45 minutes. Primer extension for sequencing reaction without

footprinted ribozyme was performed in a same manner with the addition of each ddNTP. After primer extension, RNA was degraded by alkaline hydrolysis with NaOH at 95˚C for 3 minutes. The sample was neutralized by adding HCl, and fluorescently labeled cDNA was ethanol precipitated with sodium acetate. cDNA was washed with 70% ethanol once and resuspended in water and size-standard fragments with Beckman WellRED® D1 dye (Beckman). Cy5-labeled cDNA and size-standard mix were separated by capillary electrophoresis in a Beckman CEQ8000 (Beckman). Data were processed with Capillary Automated Footprinting Analysis (CAFA) software.[22] Data were normalized with the average of all peaks after removing reverse transcriptase dependent stops. Peaks of cDNA were then aligned with the RNA sequences as determined by the separate sequencing reactions performed in parallel.

Appendix

The dimerization of 0.5 μM at the near-physiological condition did not approaching to the same end point and the same rate as the dimer dissociation at 0.5 μM. (See Figure 2.5B) Thus, I repeated the experiment to acquire an updated result. However, due to technical issues, body labeled ribozyme was used as the 3'-tail deletion experiment was done. The dimerization rate in the second phase (0.003 min^{-1}) was a lot slower than that of the previous experiment (0.02 min^{-1}). (**Figure A.1**) The similar weaker binding with 7-fold increase in K_d from previous experiments was observed for the 3'-tail deletion experiment. (See Chapter 2.5) The possible reason of this discrepancy was not understood, and a further investigation is required.

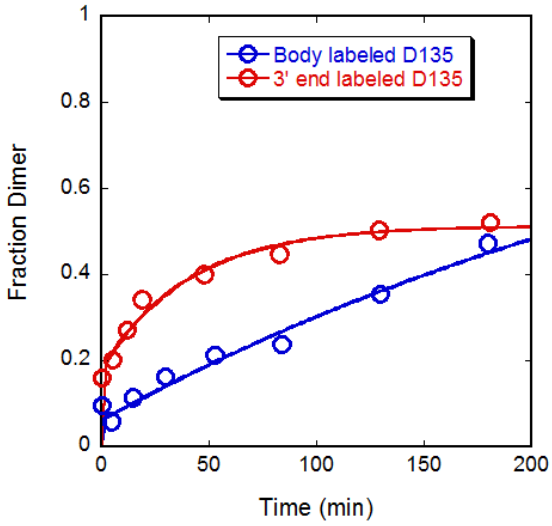

Figure A.1 Dimerization at the near-physiological condition with differently prepared D135 ribozymes

References

1. Lambowitz, A. M.; Zimmerly, S., Group II introns: mobile ribozymes that invade DNA. *Cold Spring Harb Perspect Biol* 2011, *3* (8), a003616.

2. Toor, N.; Keating, K. S.; Taylor, S. D.; Pyle, A. M., Crystal structure of a self-spliced group II intron. In *Science*, United States, 2008; Vol. 320, pp 77-82.

3. Swisher, J.; Duarte, C. M.; Su, L. J.; Pyle, A. M., Visualizing the solvent-inaccessible core of a group II intron ribozyme. *EMBO J* 2001, *20* (8), 2051-61.

4. Qin, P. Z.; Pyle, A. M., Stopped-flow fluorescence spectroscopy of a group II intron ribozyme reveals that domain 1 is an independent folding unit with a requirement for specific Mg2+ ions in the tertiary structure. In *Biochemistry*, United States, 1997; Vol. 36, pp 4718-30.

5. Swisher, J. F.; Su, L. J.; Brenowitz, M.; Anderson, V. E.; Pyle, A. M., Productive folding to the native state by a group II intron ribozyme. In *J Mol Biol*, 2002 Academic Press.: England, 2002; Vol. 315, pp 297-310.

6. Su, L. J.; Brenowitz, M.; Pyle, A. M., An alternative route for the folding of large RNAs: apparent two-state folding by a group II intron ribozyme. In *J Mol Biol*, England, 2003; Vol. 334, pp 639-52.

7. Su, L. J.; Waldsich, C.; Pyle, A. M., An obligate intermediate along the slow folding pathway of a group II intron ribozyme. In *Nucleic Acids Res*, England, 2005; Vol. 33, pp 6674-87.

8. Fedorova, O.; Waldsich, C.; Pyle, A. M., Group II intron folding under near-physiological conditions: collapsing to the near-native state. In *J Mol Biol*, England, 2007; Vol. 366, pp 1099-114.

9. Del Campo, M.; Tijerina, P.; Bhaskaran, H.; Mohr, S.; Yang, Q.; Jankowsky, E.; Russell, R.; Lambowitz, A. M., Do DEAD-box proteins promote group II intron splicing without unwinding RNA? In *Mol Cell*, United States, 2007; Vol. 28, pp 159-66.

10. Potratz, J. P.; Del Campo, M.; Wolf, R. Z.; Lambowitz, A. M.; Russell, R., ATP-dependent roles of the DEAD-box protein Mss116p in group II intron splicing in vitro and in vivo. In *J Mol Biol*, 2011 Elsevier Ltd: England, 2011; Vol. 411, pp 661-79.

11. Waldsich, C.; Pyle, A. M., A folding control element for tertiary collapse of a group II intron ribozyme. In *Nat Struct Mol Biol*, United States, 2007; Vol. 14, pp 37-44.

12. Steiner, M.; Karunatilaka, K. S.; Sigel, R. K.; Rueda, D., Single-molecule studies of group II intron ribozymes. In *Proc Natl Acad Sci U S A*, United States, 2008; Vol. 105, pp 13853-8.

13. Putnam, C. D.; Hammel, M.; Hura, G. L.; Tainer, J. A., X-ray solution scattering (SAXS) combined with crystallography and computation: defining accurate macromolecular structures, conformations and assemblies in solution. In *Q Rev Biophys*, England, 2007; Vol. 40, pp 191-285.

14. Russell, R.; Millett, I. S.; Doniach, S.; Herschlag, D., Small angle X-ray scattering reveals a compact intermediate in RNA folding. *Nat Struct Biol* 2000, *7* (5), 367-70.

15. Das, R.; Kwok, L. W.; Millett, I. S.; Bai, Y.; Mills, T. T.; Jacob, J.; Maskel, G. S.; Seifert, S.; Mochrie, S. G.; Thiyagarajan, P.; Doniach, S.; Pollack, L.; Herschlag, D., The fastest global events in RNA folding: electrostatic relaxation and tertiary collapse of the Tetrahymena ribozyme. In *J Mol Biol*, England, 2003; Vol. 332, pp 311-9.

16. Russell, R.; Jarmoskaite, I.; Lambowitz, A. M., Toward a molecular understanding of RNA remodeling by DEAD-box proteins. In *RNA Biol*, 2012; Vol. 10.

17. Wan, Y.; Mitchell, D., 3rd; Russell, R., Catalytic activity as a probe of native RNA folding. In *Methods Enzymol*, 2009 Elsevier Inc: United States, 2009; Vol. 468, pp 195-218.

18. Mortimer, S. A.; Weeks, K. M., Time-resolved RNA SHAPE chemistry. *J Am Chem Soc* 2008, *130* (48), 16178-80.

19. Huang, Z.; Szostak, J. W., A simple method for 3'-labeling of RNA. In *Nucleic Acids Res*, England, 1996; Vol. 24, pp 4360-1.

20. Grohman, J. K.; Del Campo, M.; Bhaskaran, H.; Tijerina, P.; Lambowitz, A. M.; Russell, R., Probing the mechanisms of DEAD-box proteins as general RNA chaperones: the C-terminal domain of CYT-19 mediates general recognition of RNA. *Biochemistry* 2007, *46* (11), 3013-22.

21. Tijerina, P.; Mohr, S.; Russell, R., DMS footprinting of structured RNAs and RNA-protein complexes. In *Nat Protoc*, England, 2007; Vol. 2, pp 2608-23.

22. Mitra, S.; Shcherbakova, I. V.; Altman, R. B.; Brenowitz, M.; Laederach, A., High-throughput single-nucleotide structural mapping by capillary automated footprinting analysis. In *Nucleic Acids Res*, England, 2008; Vol. 36, p e63.